Cell Reports
Resource

Mapping of Mitochondrial RNA-Protein Interactions by Digital RNase Footprinting

Ganqiang Liu,[1,2] Timothy R. Mercer,[1,2] Anne-Marie J. Shearwood,[3] Stefan J. Siira,[3] Moira E. Hibbs,[3] John S. Mattick,[1,4] Oliver Rackham,[3] and Aleksandra Filipovska[3,*]
[1]Garvan Institute of Medical Research, Sydney NSW 2010, Australia
[2]Institute for Molecular Bioscience, The University of Queensland, Brisbane QLD 4072, Australia
[3]Western Australian Institute for Medical Research, Centre for Medical Research and School of Chemistry and Biochemistry, The University of Western Australia, Perth WA 6000, Australia
[4]St Vincent's Clinical School and the School of Biotechnology and Biomolecular Sciences, The University of New South Wales, Sydney NSW 2052, Australia
*Correspondence: aleksandra.filipovska@uwa.edu.au
http://dx.doi.org/10.1016/j.celrep.2013.09.036

SUMMARY

Human mitochondrial DNA is transcribed as long polycistronic transcripts that encompass each strand of the genome and are processed subsequently into mature mRNAs, tRNAs, and rRNAs, necessitating widespread posttranscriptional regulation. Here, we establish methods for massively parallel sequencing and analyses of RNase-accessible regions of human mitochondrial RNA and thereby identify specific regions within mitochondrial transcripts that are bound by proteins. This approach provides a range of insights into the contribution of RNA-binding proteins to the regulation of mitochondrial gene expression.

INTRODUCTION

Mitochondria appear to possess very few transcription factors, but rather have a wide range of RNA-binding proteins that control gene expression at the posttranscriptional level (Falkenberg et al., 2007; Rackham et al., 2012). The mitochondrial genome is transcribed as long polycistronic transcripts that are subsequently cleaved and processed into individual mRNAs (Brzezniak et al., 2011; Holzmann et al., 2008; Sanchez et al., 2011; Ojala et al., 1981). Recent sequencing of the human mitochondrial transcriptome has revealed previously unexpected complexities of mitochondrial RNAs and identified new transcripts (Mercer et al., 2011). The large variation observed in mature mitochondrial transcripts has provided evidence that regulation of RNA processing, maturation, stability, translation, and degradation orchestrated by mitochondrial RNA-binding proteins play a major role in mitochondrial gene expression. This indicates that posttranscriptional mechanisms have assumed a pre-eminent role in mammalian mitochondrial gene regulation and expression (Rackham et al., 2012) and that achieving a profile of their interactions with mitochondrial RNAs will provide regulatory insights akin to transcription factor binding in the nuclear genome (Hesselberth et al., 2009). Here, we develop a digital RNase footprinting method that provides a global profile of RNA-protein interactions in human mitochondria and permits the investigation of posttranscriptional regulation.

RESULTS

Identification of Footprints on Mitochondrial RNAs

To identify footprints of proteins bound to mitochondrial RNAs, we treated isolated mitochondrial preparations with three endoribonucleases with different cleavage specificities (Figure 1A): RNase A, which cleaves single-stranded RNA after pyrimidine nucleotides; RNase T1, which cleaves single-stranded RNA after guanine residues; and RNase V1, which is a sequence-independent endonuclease that cleaves double-stranded RNAs. A mock-digested mitochondrial preparation was used as an accompanying control. Following the alignment and normalization of data sets to the mitochondrial genome, the site and frequency of RNase A, T1, and V1 cleavage in each data set were assigned to the position immediately upstream of the 5′ nucleotide of each read. A normalized cleavage score (C score) was ascribed to each nucleotide across the mitochondrial genome on all data sets (Experimental Procedures). By comparison to matched control digestions of purified mitochondrial RNA, a RNA footprint detection algorithm identified significant contiguous sites with a lower C score than their flanking regions. These represent footprints within mitochondrial transcripts protected from endonuclease cleavage by mitochondrial RNA-binding proteins (Figure S1A).

In total, we identified 88 distinct footprints, 33 within mRNAs, 8 from rRNAs, and 7 within tRNAs. The majority of footprints are in specific regions of mitochondrial mRNAs (Figure 1B). We found that the remaining 40 footprints were in transcription regulatory sites within the D loop and in noncoding transcripts encoded by the light strand of the mitochondrial genome. The positioning of footprints within regions of noncoding transcripts indicate a role for proteins in their biogenesis or degradation (Rackham et al., 2011).

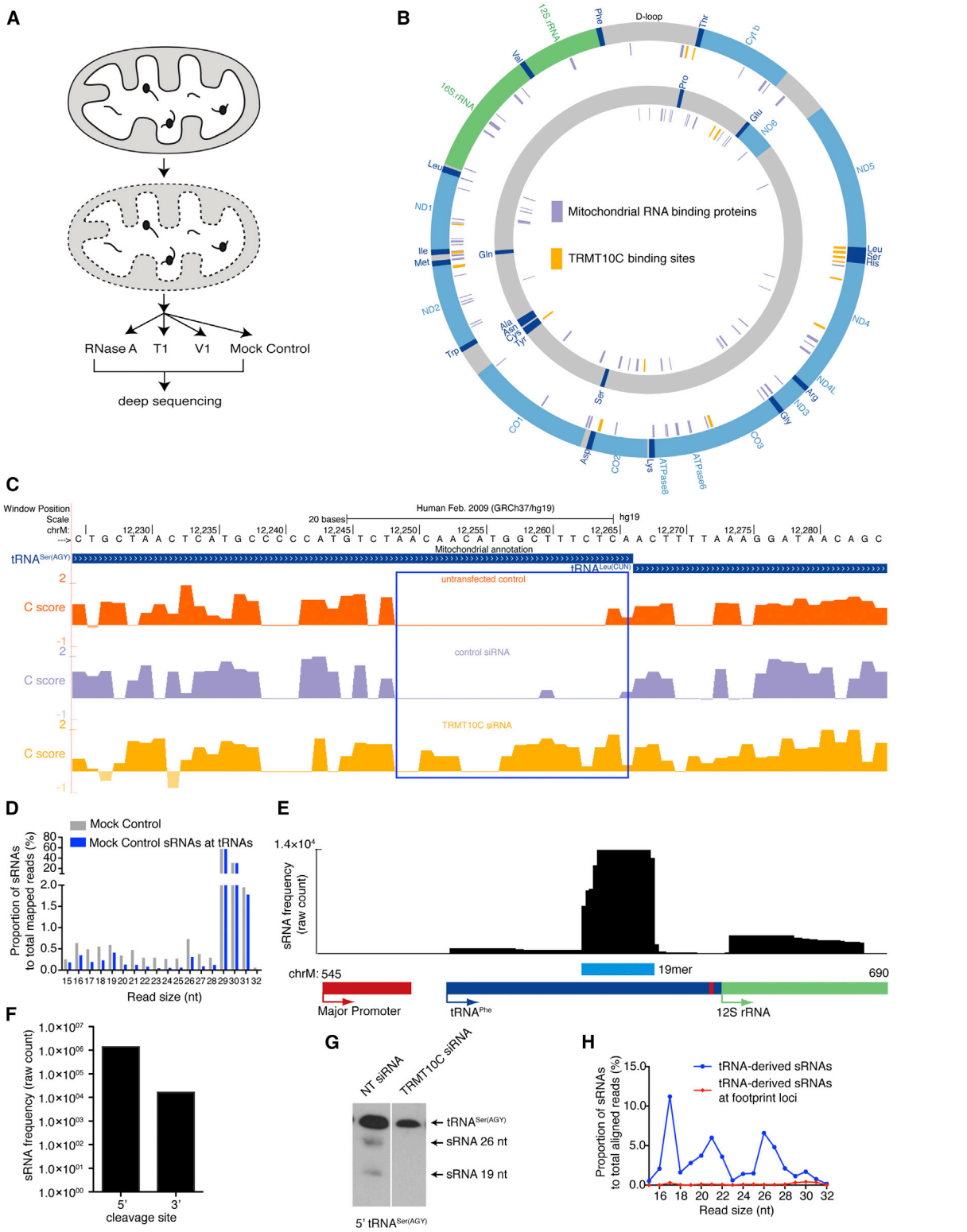

Figure 1. Mapping of Mitochondrial RNA-Protein Interactions and Small RNAs

(A) Schematic illustrating the method for mapping mitochondrial RNA-protein interactions by digital RNase footprinting.

(B) The identified mitochondrial RNA-binding protein footprints are shown in the mitochondrial transcriptome, including those of the TRMT10C protein. The outside and inner circles show mitochondrial genes on the heavy and light strand, respectively.

(legend continued on next page)

The digital RNase footprinting provides a global profile of protein interactions with the mitochondrial transcriptome. To provide insight into the identity of specific proteins interacting with the transcriptome, we performed small interfering RNA (siRNA) knockdown of the mitochondrial RNase P protein 1 (MRPP1), recently renamed tRNA methyltransferase 10 C (TRMT10C), one of the components of the RNase P complex required for cleavage of the 5′ ends of mitochondrial tRNAs (Holzmann et al., 2008), and determined its depletion in cells to be over 95% by quantitative RT-PCR and immunoblotting (Figure S1B). To identify TRMT10C footprints, we compared the data sets where TRMT10C was knocked down to data sets where mitochondria were treated with control siRNAs. We identified 17 unique footprints (Table S1) that were specifically absent from TRMT10C-knockdown mitochondrial data sets. These footprints predominantly reside within mitochondrial tRNAs, such as that found at the 3′ end of $tRNA^{Ser(AGY)}$ (MT-TS2), which is the 5′ end of $tRNA^{Leu(CUN)}$ (MT-TL2) (Figure 1C). Notably, this footprint encompasses the TΨC loop of $tRNA^{Ser(AGY)}$ and this region of tRNAs has been shown recently to be protected by the mitochondrial RNase P in *Arabidopsis*, suggesting that there is an evolutionarily conserved binding mode for tRNA 5′ processing enzymes (Gobert et al., 2013).

Recently, the presence of a noncoding small RNA (sRNA) population was identified in human mitochondria (Mercer et al., 2011). In our mock-digested mitochondrial lysates, we identified sRNAs ranging from 15 to 32 nt in size and representing 95.8% (Table S2) of the total reads aligned to the mitochondrial genome. Most identified sRNAs align to mitochondrial tRNA genes and belong to distinct size classes (Figure 1D). The majority of the 19 nt class of sRNAs aligned to $tRNA^{Phe}$ (MT-TF, positions 612∼631 of the heavy strand) (Figure 1E). This region lies immediately downstream of the major heavy strand promoter, and these sRNAs likely represent the products of abortive transcription initiation by the mitochondrial RNA polymerase (Falkenberg et al., 2007). The remaining sRNAs consist of two distinct species of sRNAs associated with mitochondrial tRNA genes, one immediately downstream of the 5′ cleavage site of tRNAs and a second less abundant species immediately downstream of the 3′ cleavage site of tRNAs (Figure 1F), that vary in size (Figure S2). The expression of the two mitochondrial tRNA-derived sRNA species was not correlated to each other, suggesting that they are generated by independent mechanisms, likely by tRNA processing enzymes. For example, we can detect the presence of sRNAs that align to the 5′ end $tRNA^{Ser(AGY)}$ in cells by northern blotting and show that knockdown of TRMT10C in cells decreased their abundance and that of the mature $tRNA^{Ser(AGY)}$ (Figure 1G), suggesting that the mitochondrial RNase P plays a role in the generation of sRNAs in mitochondria.

Mining of next-generation data sets from *Arabidopsis* and rice chloroplast genomes has identified sRNAs as potential footprints of RNA-binding proteins (Ruwe and Schmitz-Linneweber, 2012; Zhelyazkova et al., 2012). The majority of the identified protein footprints are produced from noncoding regions in the chloroplast genome as well as from 5′ and 3′ ends of mRNAs thought to be regulated by the sequence-specific family of PPR RNA-binding proteins (Ruwe and Schmitz-Linneweber, 2012; Zhelyazkova et al., 2012). We integrated our previous small RNA sequencing data set (Mercer et al., 2011) with the data sets from the endonuclease-treated samples, finding only a small number of the identified sRNAs produced from the human mitochondrial transcriptome overlap with RNA-binding protein footprints (Figure 1H). This suggests that most sRNAs are free to take part in intermolecular RNA-RNA interactions and may have regulatory roles in mitochondrial gene expression.

Identification of PPR Protein Footprints

RNA-binding proteins of the PPR family have emerged as important regulators of organelle gene expression and consequently cell health (Rackham and Filipovska, 2012; Schmitz-Linneweber and Small, 2008). These proteins are similar to the PUF and TALE proteins in that they are predicted to have a sequence-specific mode of nucleic acid recognition (Boch et al., 2009; Filipovska and Rackham, 2012; Moscou and Bogdanove, 2009; Wang et al., 2002). Therefore, there is considerable interest in identifying their RNA targets to understand better their role in RNA metabolism or to use them in biotechnology for targeting specific RNAs of interest. Here, we used RNase digital footprinting to identify binding sites of the mammalian PPR protein, pentatricopeptide repeat domain protein 1 (PTCD1), previously found to affect mitochondrial RNA metabolism (Sanchez et al., 2011; Rackham et al., 2009). We identified five PTCD1-specific RNA footprints in samples from cells where this protein was knocked down using siRNAs, relative to controls. Examples of PTCD1 footprints in $tRNA^{His}$ and $tRNA^{Ile}$ are shown in Figures 2A and 2B. We investigated the interaction between the identified RNA targets with PTCD1 in vitro using an RNA electrophoretic mobility shift assay (EMSA) (Figure 2C). The binding of the identified RNA targets to PTCD1 compared to a scrambled RNA control validated the specificity of this protein for these targets. This suggests that the RNase digital footprinting method combined with specific siRNA knockdown can be used to effectively predict the targets for RNA-binding proteins of interest.

Protein Footprints upon Stalled Mitochondrial Translation

Protein translation within mitochondria has diverged significantly from translation in the cytoplasm and prokaryotes (Suzuki et al., 2001a, 2001b) and is still poorly understood. To examine the

(C) The footprints of TRMT10C at the 3′ end of mitochondrial $tRNA^{Ser(AGY)}$ and the 5′ end of $tRNA^{Leu(CUN)}$ are shown at a single-nucleotide resolution.
(D) A histogram showing the proportion of sRNAs 15–32 nt in size and sRNAs that align to tRNA loci relative to total mapped reads.
(E) The 19 nt sRNA class aligns predominantly to the 5′ end of the $tRNA^{Phe}$ locus and is likely a product of abortive transcription.
(F) The proportion of tRNA-derived sRNAs that align to the 5′ and 3′ cleavage sites of mitochondrial tRNAs.
(G) Northern blot of $tRNA^{Ser(AGY)}$ showing the presence of sRNA in control siRNA treated mitochondria that are decreased when the mitochondrial RNase P protein TRMT10C is knocked down in cells.
(H) Limited correlation between the tRNA-derived sRNAs and identified RNA-binding footprints.

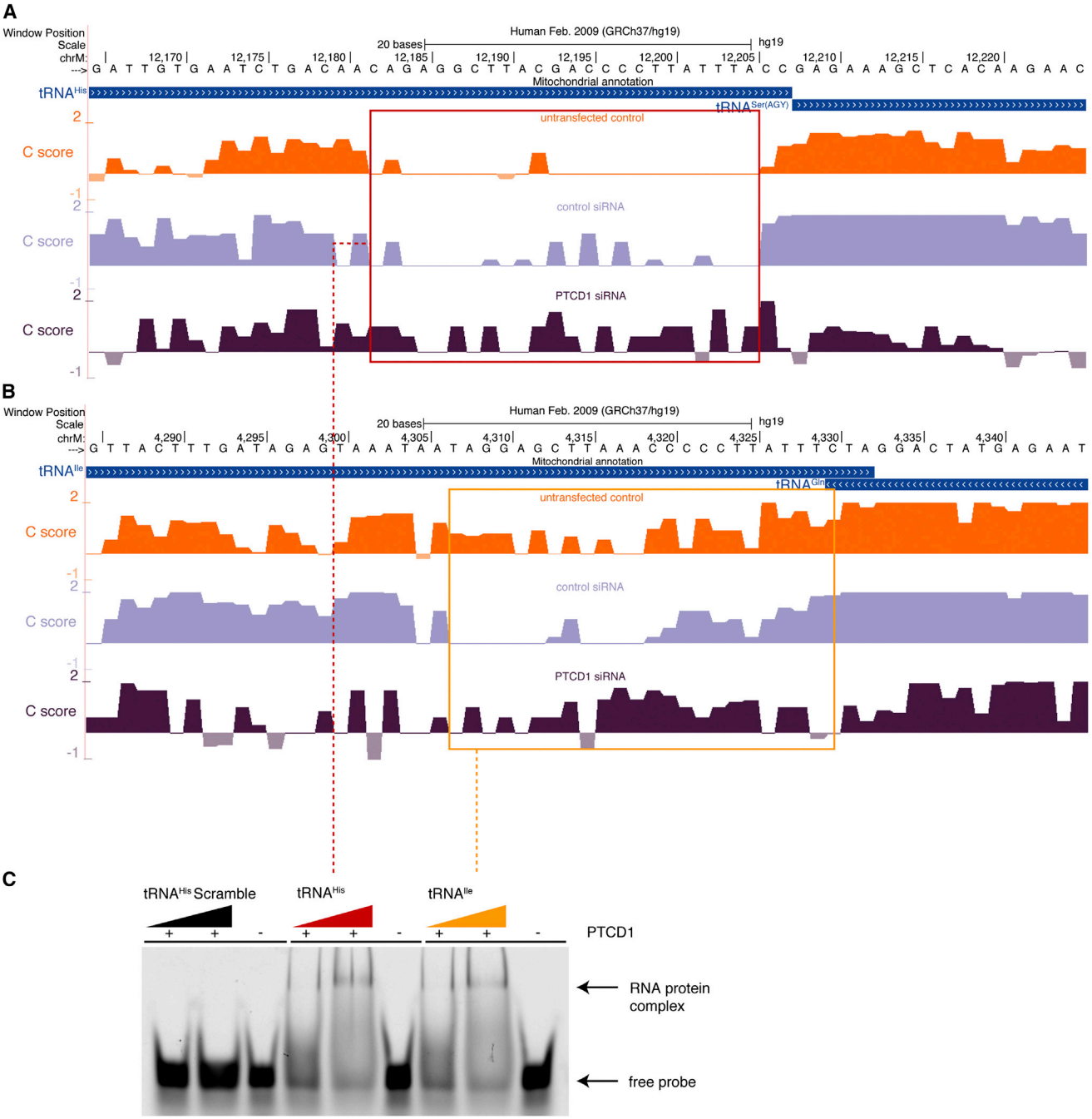

Figure 2. Identification of PTCD1 Footprints on Mitochondrial RNAs

(A and B) Specific PTCD1 protein footprints are shown at the 3′ ends of $tRNA^{His}$ (A) and $tRNA^{Ile}$ (B).

(C) An RNA EMSA shows specific in vitro binding of purified PTCD1 protein with its RNA targets identified in (A) and (B) compared to control RNA.

translational regulation of mRNAs, we treated cells with chloramphenicol to stall mitochondrial translation and performed RNA footprinting analyses. We compared data sets from mitochondria treated in the presence and absence of chloramphenicol to identify 270 footprints that were protected from endonuclease cleavage as a result of inhibiting translation. We identified 124 protein footprints (from the total of 270) that were within mitochondrial mRNAs, of which 22 were 25–35 nt in length and were recognized as mitochondrial ribosome stalling sites or mitoribosome footprints (Figure 3A). An example of a mitochondrial ribosomal footprint in MT-CO1 mRNA during translational stalling is shown in Figure 3B. The ribosome footprints were not enriched at start codons of mitochondrial mRNAs, suggesting that ribosome stalling induced by chloramphenicol may be

attributed to the downstream secondary structure. The other 102 protected sites in mitochondrial mRNAs are likely RNA-binding protein footprints that are transiently associated with mRNAs between rounds of translation. The remaining 146 protein footprints from the total 270 identified were in noncoding RNAs: 36 in rRNAs, 10 in tRNAs, and 7 in the D loop, as well as 85 in transcripts encoded by the light strand and 8 in noncoding regions of the heavy strand. Interestingly, we identified 9 ribosomal footprints in transcripts encoded by the light strand, suggesting that mitochondrial ribosomes may indiscriminately scan or initiate translation of RNAs that have cryptic start codons.

To understand the cause for the ribosomal stalling at specific regions in mitochondrial mRNAs, we investigated the correlation between the 22 identified mitoribosome footprints and RNA secondary structure. Regions within mitochondrial transcripts that are immediately upstream and downstream of the ribosomal footprints have low R scores (see Experimental Procedures), suggesting that these regions are less structured, compared to the regions further away from the footprints that are more structured and consequently have higher R scores (Figure 3C). We confirmed that the single-strand RNA structure upstream and downstream of ribosomal footprints is significant using the Wilcoxon test (see Experimental Procedures), suggesting the ribosome prevents folding of RNA immediately upstream and downstream during translation. We also considered whether the 22 identified ribosomal footprints correlate with codon usage by the mitochondrial ribosome (Jia and Higgs, 2008). We selected the lowest frequency codons in each ribosomal footprint with an average frequency of ~0.008 (Figure 3D) and compared these to the frequency of rare codons in 22 randomly selected mRNAs (Experimental Procedures). The median p value is 0.338 (Figure 3E), which suggests that ribosome stalling is not strongly influenced by the frequency of rare codons.

Digital Mapping of RNA Secondary Structures within Mitochondria

RNase cleavage coupled with deep sequencing can be used as a high-throughput method for RNA structural mapping (Fourmy and Yoshizawa, 2012). Because RNase V1 preferentially cleaves double-stranded RNAs, we used it to analyze local secondary structures of mitochondrial transcripts in our control data sets. We found that the majority of mapped reads aligned to mitochondrial rRNA genes (92.5% in mitochondrial lysates and 89.2% in purified RNA), consistent with the extensive double-stranded regions within these transcripts. To investigate the regions of mitochondrial transcripts that would be susceptible to RNase V1 cleavage, we assigned an R score to each nucleotide across the entire mitochondrial transcriptome from all data sets and identified the regions with strong secondary structure (Figure 4A; Figure S3). The R score of the mitochondrial rRNAs correlates positively with secondary structure predictions by the Matthews correlation coefficient (MCC) (Table S2; Figures S4 and S5), validating the digital approach to secondary structure prediction.

Next, we determined the average R score for mitochondrial mRNAs and found that their 5′ ends are significantly less structured (Figure 4B), corroborating previous observations (Jones et al., 2008; Montoya et al., 1981). This may facilitate the docking of the mitoribosomes onto mitochondrial mRNAs, as they lack methyl-guanosine caps or 5′ UTRs to recruit them. We investigated the structure of mitochondrial tRNAs, which differ from nuclear or bacterial tRNAs because they often miss semiconserved nucleotides and the size of the D and T loops can be reduced or absent (Giegé et al., 2012; Suzuki et al., 2011). Our digital analyses confirm previous findings that the acceptor and anticodon stems are the most structured regions in tRNAs, such as those of $tRNA^{Val}$, and the anticodon loop is the least structured (Giegé et al., 2012) (Figure 4C). Moreover, we have provided a method for investigating the unusual structures of mitochondrial tRNAs at a single-nucleotide level (Figure 4D), which has previously proven challenging.

DISCUSSION

The analyses of transcript structure and RNA-protein interactions with single-nucleotide resolution comprises a powerful approach to provide insight into the structures of mitochondrial RNAs and how they are regulated by RNA-binding proteins and recognized by the translation machinery. This is particularly valuable given that mammalian mitochondrial genomes cannot be investigated by targeted genetic manipulation. These methods provide valuable tools for future high-throughput secondary structure prediction of RNAs in cells and will enable the mitochondrial targets that are modified or bound by proteins to be deciphered. Furthermore, given the rapid improvements in next-generation sequencing approaches, the techniques and analyses developed here could be similarly applied to examine the roles of RNA-protein interactions in bacterial and cytoplasmic transcriptomes.

EXPERIMENTAL PROCEDURES

Mitochondrial Isolation and Treatment

Mitochondria or mitochondrial RNA were isolated from 143B cells, 143B cells treated with nontargeted control siRNAs, TRMT10C siRNAs, or PTCD1 siRNAs as described previously (Sanchez et al., 2011; Mercer et al., 2011). Knockdown of the proteins was confirmed by immunoblotting using TRMT10C, PTCD1, and porin antibodies (Figure S1B). To stall translation, cells were treated in the presence or absence of 100 $\mu g \cdot ml^{-1}$ chloramphenicol for 30 min on ice followed by a mitochondrial isolation and purification as above. Purified mitochondria (2 $mg \cdot ml^{-1}$) from control cells or cells treated with siRNAs or chloramphenicol were lysed by addition of 200 μl of lysis buffer (100 mM Tris-HCl, 100 mM NaCl, 40 mM $MnCl_2$, 2 mM dithiothreitol [pH 7.5], 0.1% Triton X-100). For chloramphenicol-treated samples, 100 $\mu g \cdot ml^{-1}$ chloramphenicol was included in all buffers prior to RNA isolation. The concentrations of the RNase A (10 U/μl), RNase T1 (0.1 U/μl), or RNase V1 (0.01 U/μl) were optimized and added to each mitochondrial lysate or purified RNA to generate 15–55 nt size fragments. All incubations were carried out at 37°C for up to 30 min and reactions were ended by addition of 700 μl Qiazol, followed by RNA isolation using the miRNeasy Mini Kit (QIAGEN).

Library Construction

RNA concentration, purity, and integrity were confirmed by BioAnalyser. The libraries were constructed using the Illumina TruSeq Small RNA Sample Prep Kit and deep sequencing of the mitochondrial small RNAs was performed by GeneWorks on an Illumina GAII according to the manufacturer's instructions with one modification: sample isolation from the PAGE gel after adaptor ligation was performed with a modified set of size markers to facilitate capture of small RNAs between 15 and 55 nt.

Mapping Sequenced Reads to Human Genome

Sequenced reads were initially trimmed of the 3′ adaptor sequence (5′-TGGA ATTCTCGGGTGCCAAGG-3′) prior to mapping to the reference human

Cell PRESS
Open ACCESS

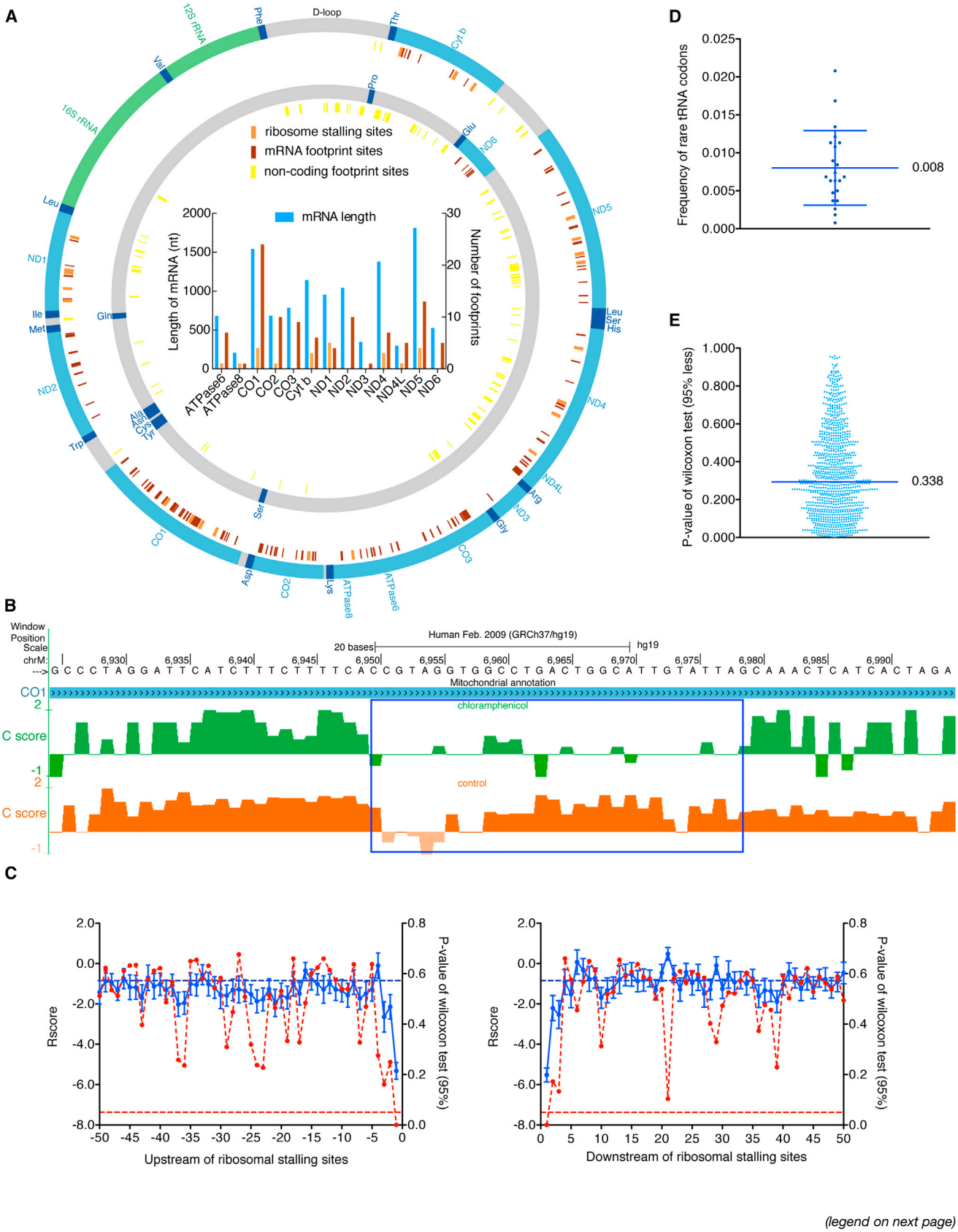

(legend on next page)

genome (hg19). Sequenced reads between 15 and 35 nt were initially aligned uniquely and exactly to the human mitochondrial genome with Bowtie (Langmead et al., 2009). The exactly and multiply mapped reads that only align to the mitochondrial genome and human nuclear mitochondrial sequences were rescued based on the NumtS track on the UCSC genome browser (Simone et al., 2011). Reads that mapped uniquely and exactly nuclear tRNA (Chan and Lowe, 2009) genes were removed. Reads that aligned to Illumina potential contaminant sequences or siRNAs we used were also discarded. Mapped reads were converted into .bed and .wig format for visualization on the UCSC genome browser (https://surf.genome.at.uq.edu.au/~uqgliu5/RnaseHub/hub.txt).

Identification of Footprints of Mitochondrial RNA-Binding Proteins

We transformed the mapped results to wig format, which represent the value of the 5′ end of sequence read coverage of each nucleotide of the mitochondrial genome. Then, we employed CPMM (counts per million mappers, reads per million in a library) to normalize different sequencing data sets. For each nucleotide, there are four normalized values from mock-treated control, RNase A, RNase T1, and RNase V1 sequencing data sets under the same experimental conditions, respectively. The RNase accessibility of each RNA nucleotide if protected by RNA-binding proteins was quantified according to the C score, the base i of C score is defined as:

$$\text{C score}_i = \log_{10}\left(\frac{\max(A_{i+1}, T1_{i+1}, V1_{i+1}) + 1}{\text{Untreated}_{i+1} + 1}\right),$$

where $A_{(i+1)}$,$T1_{(i+1)}$,$V1_{(i+1)}$ and $\text{Untreated}_{(i+1)}$ are the number of times the nucleotide immediately downstream to the inspected nucleotide was mapped as the first base of a sequence read in RNase V1-, A-, and T1-treated and untreated samples, respectively.

The footprint detection algorithm (Figure S1A) searches continuous nucleotides (8–40 nt), whose C score is lower than the average of left and right flanking nucleotides (3 nt), and we defined them as the central or core footprinting region. A central footprinting region is determined according to an F score:

$$\text{F score} = \frac{10^C}{10^L} + \frac{10^C}{10^R},$$

where C = the average C score of the central footprinting component, L = the average C score of the left flanking component, and R = the average C score of the right flanking component. For each footprint, we first calculated its F $\text{score}_{(experiment)}$ and the F score for the equivalent control data at the region, assigned it as F $\text{score}_{(control)}$; second, we divided the F $\text{score}_{(control)}$ by the F $\text{score}_{(experiment)}$ and performed a log2 transformation to yield the fold change of F score between the experimental and control conditions. To estimate if the F score fold change is significant for a footprint, we built an empirical null model by shuffling the footprints' loci. For the candidate footprint locus, the C $\text{score}_{(control)}$ must be greater than the C $\text{score}_{(experiment)}$ and the F score fold change is filtered to achieve an expected 5% false discovery rate (FDR) relative to a score obtained by random shuffling of footprints 1,000 times, as described previously (Chen et al., 2010). We employed in-house perl, awk shell, and R scripts to search for footprints. We randomly selected 22 control regions from mitochondrial mRNAs, unrelated to the identified footprints, and shuffled them 1,000 times. For each upstream or downstream nucleotide, we employed the Wilcoxon test (95% confidence level of the interval) to compare the ribosomal footprint R score to random sites and calculated an average p value from the 1,000 tests.

Northern Blotting

Northern blotting of sRNAs was carried out as described before (Pall and Hamilton, 2008), and the sRNAs were detected with biotinylated probes as described before (Rackham et al., 2009).

Purification of PTCD1 Protein

Human PTCD1 lacking its mitochondrial targeting sequence but including all PPRs predicted using TPRpred (Karpenahalli et al., 2007) (amino acids 121–632, NCBI accession number NP_056360) was subcloned into pETM30 and expressed as a fusion to an N-terminal His tag and glutathione S-transferase. Cells were lysed by sonication in 20 mM sodium phosphate (pH 8.0), 1 M NaCl, and 0.1 mM PMSF. Lysates were clarified by centrifugation and PTCD1 was purified using HIS-Select Nickel Affinity Gel according to the manufacturer's instructions (Sigma-Aldrich). The purified protein following gel filtration was dialyzed against 300 mM NaCl, 50 mM Tris-HCl (pH 7.5), and 50% glycerol before use in RNA EMSA.

RNA Electrophoretic Mobility Shift Assays

Purified PTCD1 (15 μM or 30 μM) was incubated with 40 nM fluorescein-labeled RNA oligonucleotides (Dharmacon) in 10 mM HEPES (pH 8.0), 1 mM EDTA, 50 mM KCl, 2 mM DTT, 0.1 mg/ml fatty acid-free BSA, and 0.02% Tween-20 at room temperature for 30 min. The following RNA sequences were used: $tRNA^{His}$: 5′-(Fl)CAGAGGCUUACGACCCCUUAUUUA-3′; $tRNA^{His}$-scrambled: 5′-(Fl)GCUCAUAGACUAGUAUUCAUCGCC-3′; $tRNA^{Ile}$: 5′-(Fl)UAGGAGCUUAAACCCCCUUAUUUC-3′.

RNA oligonucleotides alone or $tRNA^{His}$-scrambled RNA oligonucleotides with PTCD1 were used as controls. At the end of the incubation, the reactions were analyzed by 10% PAGE in Tris-acetate-EDTA and fluorescence was detected using a Typhoon FLA 9500 biomolecular imager (GE).

Correlation of R Score and rRNA Secondary Structure

R score was defined to quantify the probability of each nucleotide to form a paired secondary structure. The base i is defined as

$$\text{R score}_i = \log_2\left(\frac{V1_{i+1} + 1}{\max(A_{i+1}, T1_{i+1}) + 1}\right),$$

where $V1_{(i+1)}$, $A_{(i+1)}$ and $T1_{(i+1)}$ are the number of times the nucleotide immediately downstream to the inspected nucleotide was mapped as the first base of a sequence read in RNase V1-, A-, and T1-treated samples, respectively. We adopted the MCC to measure the correlation between the R score and rRNA secondary structure. The secondary structure model of human mitochondrial 12S rRNA was derived from the CRW database (Cannone et al., 2002), including +Pseudoknots templates. The secondary structure model of human mitochondrial 16S rRNA was derived from previous studies (Mears et al., 2006; Seibel et al., 2008).

$$\text{Unpaired predictive value} = \text{TP}/(\text{TP} + \text{FP})$$

$$\text{Paired predictive value} = \text{TN}/(\text{FN} + \text{TN})$$

Figure 3. Identification of Mitochondrial Ribosome Stalling Footprints

(A) Mitochondrial protein footprints and ribosome stalling sites are shown across the whole transcriptome when mitochondrial translation is inhibited with chloramphenicol. The histogram indicates the number of ribosome stalling sites found in mitochondrial mRNAs correlated to their length.

(B) A specific ribosomal protein footprint in the MT-CO1 transcript is shown that occurs as a result of translation inhibition by chloramphenicol treatment.

(C) The average R score of 50 nt upstream and downstream of 22 ribosomal stalling sites (left y axis); the blue dotted line −0.8444 is the average R score of all mitochondrial mRNA nucleotides in the chloramphenicol-treated data set. The red dotted line shows the average p value of 1,000 times Wilcoxon test (95% confidence level of the interval) for each nucleotide, indicating the comparison R score of each nucleotide 50 nt upstream and downstream of ribosomal footprints to that of random loci that were shuffled 1,000 times.

(D) The frequency of rare tRNA codon usage at reported ribosomal stalling sites.

(E) The 1,000 p value of Wilcoxon t (95% confidence level of the interval) test by comparison of codon usage at ribosomal footprints to random loci, shuffled 1,000 times.

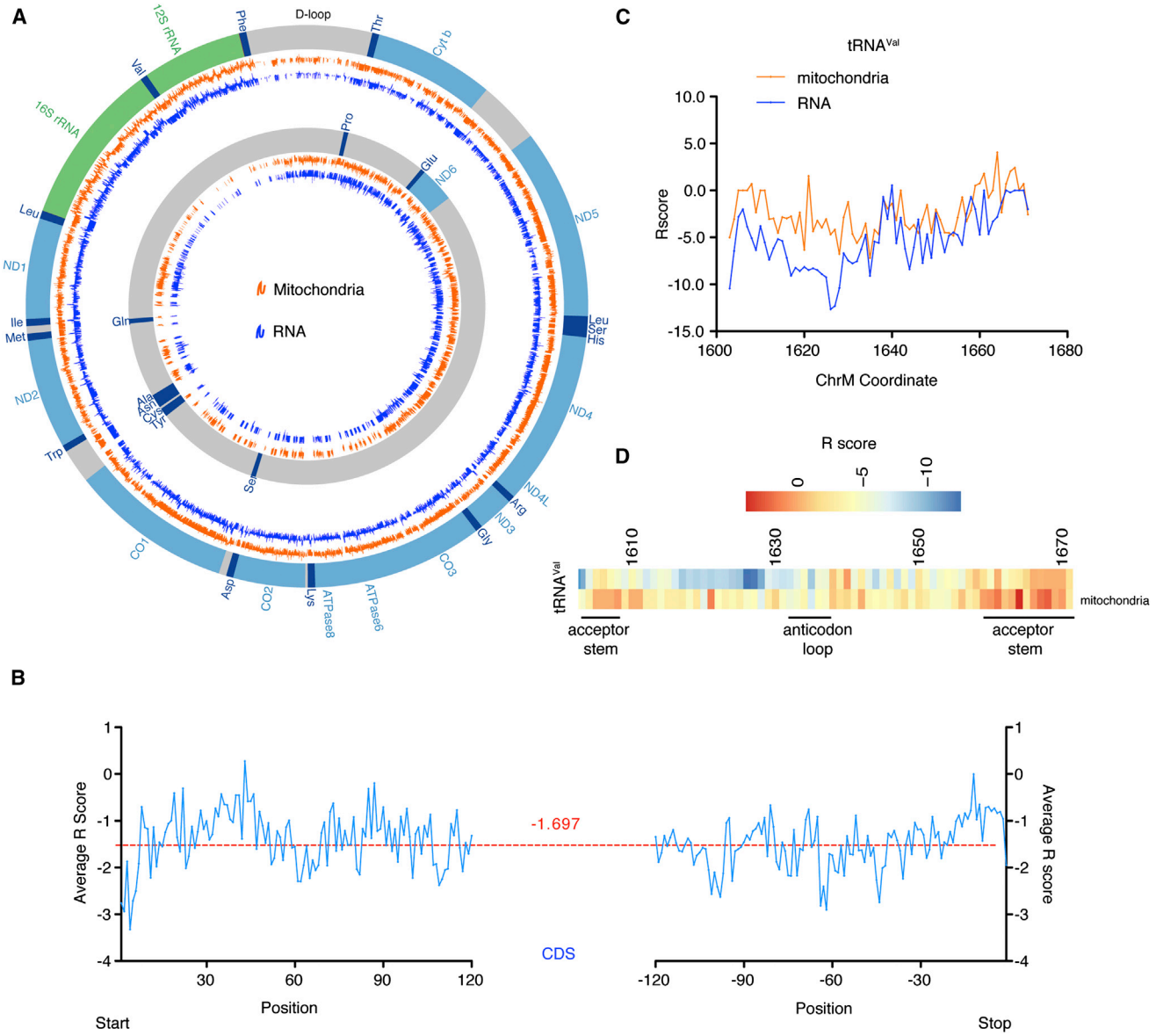

Figure 4. In Vivo Analysis of Mitochondrial RNA Secondary Structure

(A) Histogram of the R score of every nucleotide across the whole mitochondrial transcriptome from control mitochondria and its matched purified RNA data sets. From center, the outer two tracks show the R score of each nucleotide of transcripts on the mitochondrial heavy strand, while the inner two tracks correspond to the light strand. This figure was constructed using Circos (Krzywinski et al., 2009).

(B) R score across the coding sequences (CDS) of mitochondrial mRNA transcripts. Transcripts were aligned by their translational start and stop sites; the horizontal line denotes the average R score of mitochondrial CDS.

(C and D) R score across every nucleotide of $tRNA^{Val}$ from control mitochondria (C) and its matched purified RNA data sets and their heat maps (D) showing the specific loops and stems of this tRNA.

$$\text{Accuracy} = (TP + TN)/(TP + TN + FP + FN)$$

$$MCC = \frac{TP \times TN - FP \times FN}{\sqrt{(TP + FP)(TP + FN)(TN + FP)(TN + FN)}}$$

The MCC is used here to measure the quality of R score classification. A coefficient of +1 represents a perfect prediction, 0 indicates no better than random prediction, and −1 indicates disagreement between prediction and observation.

ACCESSION NUMBERS

The Sequence Read Archive (SRA) accession number for the data reported in this paper is SRA098892.

SUPPLEMENTAL INFORMATION

Supplemental Information includes five figures and two tables and can be found with this article online at http://dx.doi.org/10.1016/j.celrep.2013.09.036.

ACKNOWLEDGMENTS

The pETM30 plasmid was a kind gift from the EMBL Protein Expression and Purification Facility. This work was supported by the Australian Research Council (Future Fellowships to A.F. and O.R.) and the National Health and Medical Research Council of Australia (Australia Fellowship 631668 to J.S.M. and Project Grants to A.F. and O.R.).

Received: June 30, 2013
Revised: September 4, 2013
Accepted: September 25, 2013
Published: October 31, 2013

REFERENCES

Boch, J., Scholze, H., Schornack, S., Landgraf, A., Hahn, S., Kay, S., Lahaye, T., Nickstadt, A., and Bonas, U. (2009). Breaking the code of DNA binding specificity of TAL-type III effectors. Science *326*, 1509–1512.

Brzezniak, L.K., Bijata, M., Szczesny, R.J., and Stepien, P.P. (2011). Involvement of human ELAC2 gene product in 3′ end processing of mitochondrial tRNAs. RNA Biol. *8*, 616–626.

Cannone, J.J., Subramanian, S., Schnare, M.N., Collett, J.R., D'Souza, L.M., Du, Y., Feng, B., Lin, N., Madabusi, L.V., Müller, K.M., et al. (2002). The comparative RNA web (CRW) site: an online database of comparative sequence and structure information for ribosomal, intron, and other RNAs. BMC Bioinformatics *3*, 2.

Chan, P.P.P., and Lowe, T.M.T. (2009). GtRNAdb: a database of transfer RNA genes detected in genomic sequence. Nucleic Acids Res. *37*(Database issue), D93–D97.

Chen, X., Hoffman, M.M., Bilmes, J.A., Hesselberth, J.R., and Noble, W.S. (2010). A dynamic Bayesian network for identifying protein-binding footprints from single molecule-based sequencing data. Bioinformatics *26*, i334–i342.

Falkenberg, M., Larsson, N.G., and Gustafsson, C.M. (2007). DNA replication and transcription in mammalian mitochondria. Annu. Rev. Biochem. *76*, 679–699.

Filipovska, A., and Rackham, O. (2012). Modular recognition of nucleic acids by PUF, TALE and PPR proteins. Mol. Biosyst. *8*, 699–708.

Fourmy, D.D., and Yoshizawa, S.S. (2012). Protein-RNA footprinting: an evolving tool. Wiley Interdiscip Rev RNA *3*, 557–566.

Giegé, R., Jühling, F., Pütz, J., Stadler, P., Sauter, C., and Florentz, C. (2012). Structure of transfer RNAs: similarity and variability. Wiley Interdiscip Rev RNA *3*, 37–61.

Gobert, A., Pinker, F., Fuchsbauer, O., Gutmann, B., Boutin, R., Roblin, P., Sauter, C., and Giegé, P. (2013). Structural insights into protein-only RNase P complexed with tRNA. Nat. Commun. *4*, 1353.

Hesselberth, J.R., Chen, X., Zhang, Z., Sabo, P.J., Sandstrom, R., Reynolds, A.P., Thurman, R.E., Neph, S., Kuehn, M.S., Noble, W.S., et al. (2009). Global mapping of protein-DNA interactions in vivo by digital genomic footprinting. Nat. Methods *6*, 283–289.

Holzmann, J., Frank, P., Löffler, E., Bennett, K.L., Gerner, C., and Rossmanith, W. (2008). RNase P without RNA: identification and functional reconstitution of the human mitochondrial tRNA processing enzyme. Cell *135*, 462–474.

Jia, W., and Higgs, P.G. (2008). Codon usage in mitochondrial genomes: distinguishing context-dependent mutation from translational selection. Mol. Biol. Evol. *25*, 339–351.

Jones, C.N., Wilkinson, K.A., Hung, K.T., Weeks, K.M., and Spremulli, L.L. (2008). Lack of secondary structure characterizes the 5′ ends of mammalian mitochondrial mRNAs. RNA *14*, 862–871.

Karpenahalli, M.R., Lupas, A.N., and Söding, J. (2007). TPRpred: a tool for prediction of TPR-, PPR- and SEL1-like repeats from protein sequences. BMC Bioinformatics *8*, 2.

Krzywinski, M., Schein, J., Birol, I., Connors, J., Gascoyne, R., Horsman, D., Jones, S.J., and Marra, M.A. (2009). Circos: an information aesthetic for comparative genomics. Genome Res. *19*, 1639–1645.

Langmead, B.B., Trapnell, C.C., Pop, M.M., and Salzberg, S.L.S. (2009). Ultrafast and memory-efficient alignment of short DNA sequences to the human genome. Genome Biol. *10*, R25.

Sanchez, M.I., Mercer, T.R., Davies, S.M., Shearwood, A.-M.J., Nygård, K.K., Richman, T.R., Mattick, J.S., Rackham, O., and Filipovska, A. (2011). RNA processing in human mitochondria. Cell Cycle *10*, 2904–2916.

Mears, J.A., Sharma, M.R., Gutell, R.R., McCook, A.S., Richardson, P.E., Caulfield, T.R., Agrawal, R.K., and Harvey, S.C. (2006). A structural model for the large subunit of the mammalian mitochondrial ribosome. J. Mol. Biol. *358*, 193–212.

Mercer, T.R., Neph, S., Dinger, M.E., Crawford, J., Smith, M.A., Shearwood, A.-M.J., Haugen, E., Bracken, C.P., Rackham, O., Stamatoyannopoulos, J.A., et al. (2011). The human mitochondrial transcriptome. Cell *146*, 645–658.

Montoya, J., Ojala, D., and Attardi, G. (1981). Distinctive features of the 5′-terminal sequences of the human mitochondrial mRNAs. Nature *290*, 465–470.

Moscou, M.J., and Bogdanove, A.J. (2009). A simple cipher governs DNA recognition by TAL effectors. Science *326*, 1501.

Ojala, D., Montoya, J., and Attardi, G. (1981). tRNA punctuation model of RNA processing in human mitochondria. Nature *290*, 470–474.

Pall, G.S., and Hamilton, A.J. (2008). Improved northern blot method for enhanced detection of small RNA. Nat. Protoc. *3*, 1077–1084.

Rackham, O., and Filipovska, A. (2012). The role of mammalian PPR domain proteins in the regulation of mitochondrial gene expression. Biochim. Biophys. Acta *1819*, 1008–1016.

Rackham, O., Davies, S.M.K., Shearwood, A.-M.J., Hamilton, K.L., Whelan, J., and Filipovska, A. (2009). Pentatricopeptide repeat domain protein 1 lowers the levels of mitochondrial leucine tRNAs in cells. Nucleic Acids Res. *37*, 5859–5867.

Rackham, O., Shearwood, A.-M.J., Mercer, T.R., Davies, S.M.K., Mattick, J.S., and Filipovska, A. (2011). Long noncoding RNAs are generated from the mitochondrial genome and regulated by nuclear-encoded proteins. RNA *17*, 2085–2093.

Rackham, O., Mercer, T.R., and Filipovska, A. (2012). The human mitochondrial transcriptome and the RNA-binding proteins that regulate its expression. Wiley Interdiscip Rev RNA *3*, 675–695.

Ruwe, H., and Schmitz-Linneweber, C. (2012). Short non-coding RNA fragments accumulating in chloroplasts: footprints of RNA binding proteins? Nucleic Acids Res. *40*, 3106–3116.

Schmitz-Linneweber, C., and Small, I. (2008). Pentatricopeptide repeat proteins: a socket set for organelle gene expression. Trends Plant Sci. *13*, 663–670.

Seibel, P.P., Di Nunno, C.C., Kukat, C.C., Schäfer, I.I., Del Bo, R.R., Bordoni, A.A., Comi, G.P.G., Schön, A.A., Capuano, F.F., Latorre, D.D., and Villani, G. (2008). Cosegregation of novel mitochondrial 16S rRNA gene mutations with the age-associated T414G variant in human cybrids. Nucleic Acids Res. *36*, 5872–5881.

Simone, D., Calabrese, F.M., Lang, M., Gasparre, G., and Attimonelli, M. (2011). The reference human nuclear mitochondrial sequences compilation validated and implemented on the UCSC genome browser. BMC Genomics *12*, 517.

Suzuki, T., Terasaki, M., Takemoto-Hori, C., Hanada, T., Ueda, T., Wada, A., and Watanabe, K. (2001a). Proteomic analysis of the mammalian mitochondrial ribosome. Identification of protein components in the 28 S small subunit. J. Biol. Chem. *276*, 33181–33195.

Suzuki, T., Terasaki, M., Takemoto-Hori, C., Hanada, T., Ueda, T., Wada, A., and Watanabe, K. (2001b). Structural compensation for the deficit of rRNA

with proteins in the mammalian mitochondrial ribosome. Systematic analysis of protein components of the large ribosomal subunit from mammalian mitochondria. J. Biol. Chem. *276*, 21724–21736.

Suzuki, T., Nagao, A., and Suzuki, T. (2011). Human mitochondrial tRNAs: biogenesis, function, structural aspects, and diseases. Annu. Rev. Genet. *45*, 299–329.

Wang, X., McLachlan, J., Zamore, P.D., and Hall, T.M. (2002). Modular recognition of RNA by a human pumilio-homology domain. Cell *110*, 501–512.

Zhelyazkova, P., Hammani, K., Rojas, M., Voelker, R., Vargas-Suárez, M., Börner, T., and Barkan, A. (2012). Protein-mediated protection as the predominant mechanism for defining processed mRNA termini in land plant chloroplasts. Nucleic Acids Res. *40*, 3092–3105.